A COMPREHENSIVE RANKING FRAMEWORK FOR ACTIVE DEBRIS REMOVAL MISSIONS CANDIDATES

Giacomo Borelli, Mirko Trisolini, Mauro Massari, and Camilla Colombo

Politecnico di Milano, 20156 Milan, Italy, Email: giacomo.borelli@polimi.it , mirko.trisolini@polimi.it, mauro.massari@polimi.it, camilla.colombo@polimi.it

ABSTRACT

Active debris removal missions are necessary to guarantee the safe and sustainable use of space resources and environment in the future. The development of priority lists describing the severity of each object in orbit to the debris environment and its evolution have been widely addressed in literature to support the candidate selection for removal missions. In this work, a comprehensive ranking framework is developed, extending the assessment of the objects' criticality also to the economical orbital resource value and the mission operations requirements based on the target state and characteristics. The developed ranking framework is aimed to support the design multiple target active debris removal missions, and to preliminary assess the reliability requirements needed for the disposal options. The scheme is applied to the low Earth orbit population and the results are discussed.

Keywords: Debris Remediation; Active Debris Removal; Index.

1. INTRODUCTION

The developments in the study of space debris and its effects on the space environment and space activities have greatly advanced in the last decades, since the pioneer study in 1978 by Kessler et al. [22]. The years of study and research brought to the space community the awareness of the importance of sustainable space operations and exploitation of space resources. In 2002, the Inter-Agency Space Debris Committee (IADC) issued a set of mitigation requirements and guidelines to limit the future generation of debris in orbit [18, 16]. On the other hand, several studies have highlighted the need of an active remediation strategy to control the debris evolution [27, 28, 36]. These studies have shown that a rate of approximately five large objects per year is required to avoid a steady increase of the debris population due to further collisions and explosions. Nowadays, with the current launch trends this need is becoming more and more compelling. Several efforts have been placed to design Active Debris Removal (ADR) missions. The e.Deorbit mission study, performed by the ESA CleanSpace Initiative was developed to de-orbit the large Earth observation satellite ENVISAT [6]. In 2020, ESA commissioned the first ADR mission to ClearSpace, to remove the VESPA adaptor from orbit. Demonstration missions have been also launched to demonstrate various operations of an ADR mission [7, 15]. Active debris removal concepts are also under development as a commercial service to large constellations fleet and other commercial entities [9, 11, 17].

While the required technological steps of an active debris removal mission and service have been taken, the economical feasibility, and the political issues of approaching objects belonging to different countries have slowed down the process of systematic ADR mission services and remediations developments.

Of great interest in the design of active debris removal missions, particularly in the context of architectures targeting multiple objects, is the selection of suitable targets. The focus of this work is placed on the priority ranking of candidates for removal in Low Earth Orbit (LEO). The population analysed is taken from the ESA DISCOS database [14], considering payload and rocket bodies. Figure 1, displaying the mass distribution of objects over semi-major axis and inclination in LEO, clearly shows several clusters of derelict objects, i.e. in the Sun Synchronous Orbit (SSO) region. However, the actual assessment of a priority list to optimise the ADR mission output is needed.

In literature several debris candidate selection methods have been proposed [29], focusing on the effect on the debris environment evolution and effects depending on the target properties, e.g. mass, collision probability. In this paper, a ranking selection framework is developed considering several impact factors for selecting appropriately an active debris removal mission candidate. The ranking method presented is aimed to be included in the future within a systematic and optimised design of ADR missions and services according to different mission requirements and desired outputs. The paper is organised with a first description and definition of the ADR index method proposed, followed by a discussion on the included subindeces. Finally, the application of the ranking scheme to the LEO objects population is presented and the results

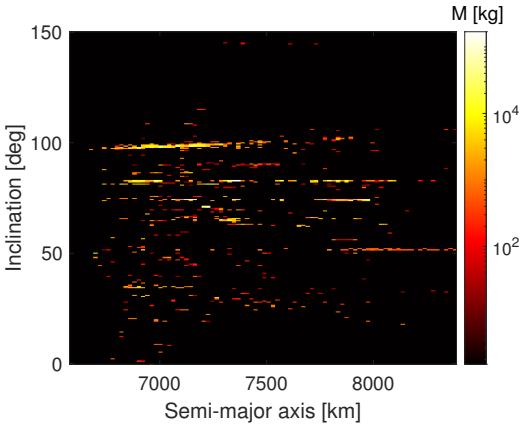

Figure 1: Mass distribution of objects in LEO, considering payload and rocket bodies from DISCOS [14].

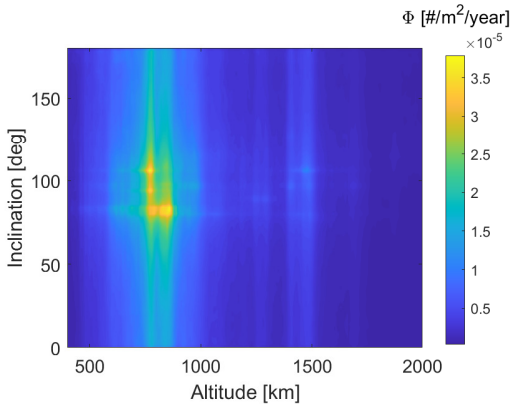

Figure 2: Debris flux grid in LEO computed with the MASTER-8 model considering objects greater than 10 cm.

are discussed.

2. ACTIVE DEBRIS REMOVAL INDEX DEFINITION

The index definition encompass four different domains of impact for an ADR mission. These impact domains are enclosed in four different sub-indices, namely the environmental, economical, operational and mission related factors of an ADR mission. Then, the ADR index is defined as a weighted sum of the four defined normalised sub-indices as follows.

$$I_{ADR} = w_{env} I_{env} + w_E I_E + w_O I_O + w_{mis} I_{mis} \quad (1)$$

The present framework developed to classify the debris objects according to their different characteristics is aimed at providing a tool to select the appropriate candidate and mission architecture for active debris removal. In fact, multiple ADR and mission are proven to be economically viable, but the target selection and sequence that minimize the cost and maximize the output is a topic of research and debate which still lacks of a systematic approach. The present framework describes and classifies the debris environment to enable a meditated choice according to the different objects properties. The future application of the present ranking and evaluation scheme is to be included in a systematic approach to optimally select mission candidates for removal.

3. ENVIRONMENTAL INDEX

As the name implies, the environmental index describe the criticality of a certain inactive object to the debris orbital environment, closely related to the benefit arising from its removal. In literature, different studies are present to quantify the environmental impact of a specific debris object. In 2009, Liou and Johnson presented a ranking method evaluating the product of mass and collision probability of objects from spatial densities and relative velocities [28]. In [38], the objects are studied considering their capability of generating fragments due to a collision. In the works of Anselmo and Pardini, the ranking proposed is based on the product of the probability of catastrophic collision with the number of fragments generated [3, 4, 5]. Similarly, Rossi et al. formulated the Criticality of Spacecraft Index (CSI) considering the spatial density of debris, orbital life time, mass and inclination factor [31]. Virgili ranked the objects considering Monte-Carlo runs and evaluating the objects which are involved in collisions using long-term propagation of the debris environment [36, 37]. In Letizia et al. [25], an an index (ECOB) is defined based on the effects of a fragmentation, simulating its evolution and the evaluating the collision probability for a set of representative targets in the LEO region of interest. In [26], the ECOB index was extended to consider also the estimation of the fragmentation risks and explosions effects.

The environmental index I_{env} used in this work is based on the previous heritage, particularly on the work of [3, 4, 5], considering the trade-off in complexity and computational expense in the evaluation. The formulation is reported in the following equations.

$$P_c \approx \Phi \cdot M \cdot life(h) \quad (2)$$

$$N_f \approx M^{0.75} \quad (3)$$

$$I_{env} = \left(\frac{\Phi}{\Phi_0}\right) \cdot \left(\frac{M}{M_0}\right)^{1.75} \cdot \left(\frac{life}{life_0}\right) \quad (4)$$

In Equation 3, Φ is the current debris flux encountered by the object, while M is the mass of the object from DISCOS database and $life$ is the orbital lifetime function. In this work, Φ is computed using the MASTER-8 environment model, considering objects with size greater than 10 cm. The size threshold selected corresponds to a catastrophic collision with impact energy of 40 J/g. For computational purposes, the flux is computed for a 2D grid in mean altitude and inclination in LEO, shown in

Figure 2, and the specific value for each LEO object is obtained through simple interpolation. The mean altitude is defined subtracting the mean Earth's equatorial radius to the semi-major axis. Mean altitude results equivalent to the constant altitude only in the case of a circular orbit. The orbital life time function is computed using the semi-analytical propagator PlanODyn developed at Politecnico di Milano [10]. A cut-off in reentry time of 200 years is set to avoid excessive weighting of high altitude objects. Equation 3 expresses the number of fragments generated from a catastrophic collision according to the NASA break-up model in adherence with [20].

The environmental index of Equation 3 is then normalized with the value corresponding to an object of 1000 kg of mass in an orbit of 800 km of altitude and 98.5 deg of inclination. The present definition results in higher values of environmental index for objects which pose an higher risk to the debris environment.

4. ECONOMICAL INDEX

The environmental index defined in the previous section represents the criticality of the presence of certain object to the near-Earth debris environment. However, the advantages from its removal from a point of view of economic exploitation of the space resources is not directly addressed. In fact, only the debris environment status is evaluated, without considering the danger that a specific debris object poses to the economic value of the specific orbital regions which occupies. To this aim, the economic resource value endangered by each debris object is quantified by assigning an index to each altitude and inclination bin, here denoted as economical index I_E.

Two different definitions of the orbital resource value index are explored and compared in this study. The general purpose of the models used is to obtain a valuable definition of the relative economical resource value for different orbital regions in LEO, rather than an accurate absolute model of the actual economical resource value of each orbital slot.

The first model is defined starting from the work in [12], where a sum of the estimated revenue value of every active satellite in each orbital bin is used. The revenue value for each satellite is estimated considering the revenue values by satellite type from the Satellite Industry Association (SIA) report [13]. In this work the orbital resource value assessment of work [12] is complemented considering the mass of each satellite as follows.

$$I_{E,1} = \sum_{k} \sum_{j \in (\Delta a, \Delta i)} \left(M_j Q_{k,j} \right) \frac{1}{Q_{tot}} \frac{1}{M_{k,tot}} \tag{5}$$

$$\overline{I}_{E,1} = \log_{10} \left(\frac{I_{E,1}}{I_{E,1_0}} \right) + 10 \tag{6}$$

In Equation 6, $Q_{k,j}$ is the estimated revenue value of the satellite k-th type assigned to the satellite j, while M_j represents its mass. $M_{k,tot}$ and Q_{tot} are respectively the total mass of satellites of the k-th type and the total revenue value of the satellite industry. The discretisation bins widths are considered 50 km and 2 deg in altitude and inclination respectively. The $I_{E,1}$ index is then normalised with the value computed for the SSO bin of 800 km of altitude and 98.5 deg of inclination and defined in a logarithmic scale, as reported in Equation 6. The computed map in mean altitude and inclination with the first model of economical resource value of the LEO orbital region is shown in Figure 3. The latter definition results in higher value of $I_{E,1}$ for higher economical resource value of the orbital bin.

The second model used to estimate the economical resource value of LEO orbital regions is based on the cumulative insured value of active satellites contained in a specific orbital bin. The insured value of the satellite present in each bin is estimated considering the correlation from reference [24], where the satellite mass is used as a proxy for its estimated insured value. The economical index formulated in this fashion considers a situation where every active satellite will be covered by insurance, and results in:

$$I_{E,2} = \sum_{j \in (\Delta a, \Delta i)} 52253 \left(M_j \right)^{0.9843} \tag{7}$$

$$\overline{I}_{E,2} = \log_{10} \left(\frac{I_{E,2}}{I_{E,2_0}} \right) + 10 \tag{8}$$

In Equation 8, M_j is the satellite mass in kg. As for the first model of economical index, the index for each bin computed with Equation 8 is then normalised with the value associated to the orbital bin of 800 km of altitude and 98.5 deg of inclination, and translated to a logarithmic scale as denoted in Equation 8. The computed map with the described second model of economical resource value is shown in Figure 4. As for the first mode, the latter definition results in higher value of $I_{E,2}$ for higher economical resource value of the orbital bin.

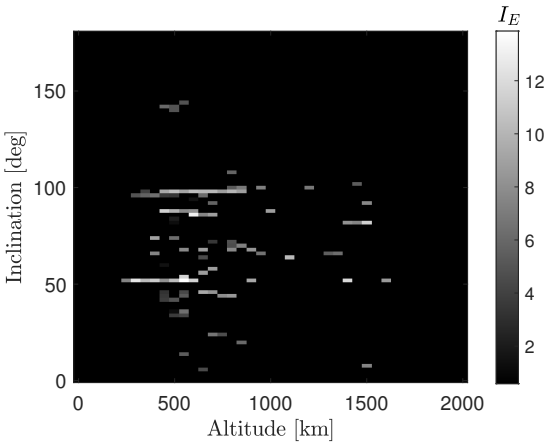

Figure 3: Logaritmic economical index $I_{E,1}$ defined with the first model of Equation 6.

Despite showing different results in terms of absolute index for each orbital bin, the two proposed models shown

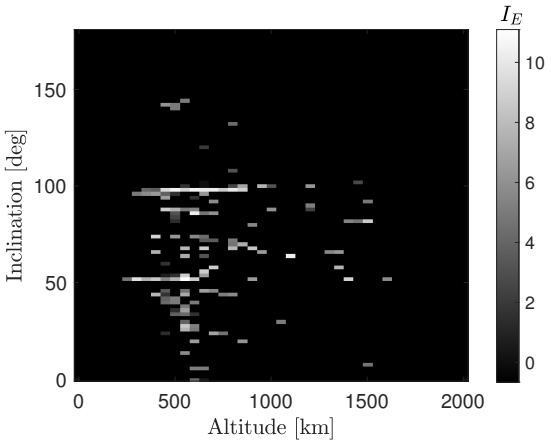

Figure 4: Logaritmic economical index $I_{E,2}$ defined with the second model of Equation 8.

in Figures3 and 4 do not greatly differ from the point of view of relative distribution of value across the LEO orbital region. The main difference identified is associated with the higher relative weighting of orbital slots containing communication satellites for the first model of Equation 6 with respect to the second model based on the estimated insured value, mainly due to the larger proxy value of revenue used for communications satellites from [13].

In this study, the orbital resource economic index selected to complement the full ADR index I_{ADR} is the one considering the first model presented in Equation 6 and Figure 3. Although, both model can be used for a preliminary relative weighting of the orbital resource value in LEO orbital regions.

5. OPERABILITY INDEX

The third sub-index composing the ADR index in Equation 1 describes the operative requirements and complications arising during the operations of approach and capture of a uncooperative target. Specifically, the operability index aims to quantify the difficulties in the approach and capture of a target based on its its physical and dynamical characteristics. Three main properties of the target are considered to influence the approach and capture phases:

- **Attitude state**: The tumbling motion of the target will require the servicer to synchronize to its motion in order to rigidly attach to the target.
- **Mass**: A massive satellite will impose more stringent constraints on the capture mechanisms employed and propellant requirements for the deorbiting.
- **Illumination conditions**: Relative sensors measurements and operations are poorly affected by difficult illumination conditions, i.e. eclipse region.

The assumption of a rigid capture method, i.e. a robotic arm, is used in the present definition considering the maturity level and feasibility of the technology for removal. For other capture methods some of the latter considerations may become inapplicable, while some may be added.

The information regarding the attitude state of each debris object is taken considering the light curve data of the objects from ground observations [19, 35, 33, 30]. From the light curve data, the apparent period can be retrieved with a Fourier analysis. Despite the apparent period does not represent directly the target absolute angular rate, it provides a reliable estimation of the entity and magnitude of a debris attitude state. Additionally, the study on the estimation of the target shape and attitude motion based on light curve data is also a active field of research [2, 8]. However, such high fidelity estimation is out of the scope of this study which mainly aims to rank and weight the debris population according to its characteristics in a relative fashion. One major issue for the fidelity of this index computation in this work is the public availability of light curve data for debris objects. Figure 5 shows the count of different attitude states in function of the mass class of objects. The mass classes are defined considering $m < 100$ kg as small, $100\ \text{kg} < M < 1000$ kg as medium and $M > 1000$ kg as large. The objects with an apparent period in the dataset has been labelled as rotating, while in the cases where no variation of the light curve magnitude is detectable and/or associated with a clear period, the objects are labelled as stable. Nonetheless, it can be noted that only 1787 out of 6094 objects of the whole database have publicly available light curve data. Considering only the objects in LEO, this number decrease to 968 out of 2597 objects. The data sources analysed to retrieve the light curve data are reported in Table 1. It should be noted that complementing this data availability will improve the operability index computation fidelity.

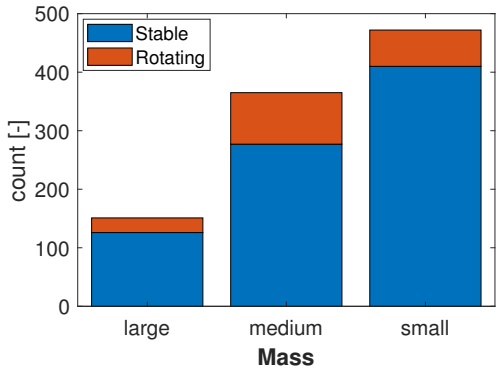

Figure 5: Count of different attitude states for the defined mass classes in LEO. Data from the sources of Table 1.

The operability index is defined as a product of different impact functions which enclose the latter considerations.

Table 1: Database of light curve to retrieve the apparent angular rate informations, where N/A stands for no data publicly available, either in raw format for light curve or in processed format as apparent period.

Source		Comment
MMT telescope [1]	Partial	No CIS data
AIUB (ZIMLAT) [34]	N/A	Only papers
Slovak AG070 [32]	Partial	Only app. per.
Odessa Obs. [21, 23]	N/A	Only L.C. plots

The index is formulated as follows:

$$I_O = P_{ecl} S_f \left(\frac{a_{s0}(L, \omega_f)}{a_s(L, \omega_f)} \right) \left(\frac{M_0 - M}{M_0} \right) \qquad (9)$$

where

$$a_s(L, \omega_f) = L\omega_f^2 \qquad \text{with} \quad \omega_\mathrm{f} = \frac{\omega_\mathrm{a}}{3 \text{ deg/s}} \qquad (10)$$

The function $a_s(L, \omega_f)$ of Equation 10 estimates of the acceleration levels required to obtain a full synchronization of the chaser with the target tumbling motion at a certain safe distance L. The safe distance L is defined as twice the maximum dimension of the debris object, from DISCOS database [14]. The ω_f factor is computed from the apparent apparent angular rate data. For the objects which do not show in the light curve data any periodicity, labelled as stable, the constant $\omega_a = 1$ deg/s is taken. On the other hand, for the objects with no available light curve data, the constant value of $\omega_a = 3$ deg/s is considered. The function definition is based on the simple consideration of compensation of the centrifugal acceleration in the rotating target body reference frame. This definition is verified with a simulation model that implements a fly-around control with a linear quadratic tracking controller considering different station keeping distances and target attitude states. The simulated results for the mean acceleration required in the synchronization for a grid of values of angular rate and distances are shown in the surface of Figure 6, together with the fitted data (black markers) of the function $a_s(L, \omega_f)$. It can be noted a slight difference for high distances L and angular rates, most likely due to other perturbing relative accelerations, i.e. Coriolis, and the induced precession motion of the target imposed during the multiple simulations performed. Nonetheless, the simple formulation of the function $a_s(L, \omega_f)$ shows a satisfactory agreement with the simulated results the function definition and assumptions. In Equation 9, the a_s function is considered at the denominator resulting in an higher value of I_O for slower tumbling objects. Additionally, a_s is normalised with the value corresponding to a $\omega = 3$ deg/s and $L = 2$ m.

In Equation 9, S_f represents a shape factor between 0 and 1 classifying complex shapes to be captured from the shapes property contained in the DISCOS database. Moreover, the term P_{ecl} represents the average percentage of orbit in eclipse during a one year simulation, estimating the probability for each object to encounter a poor

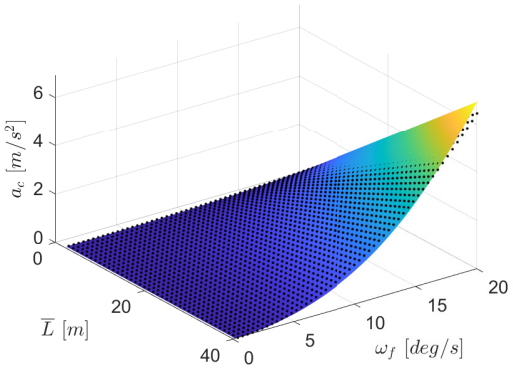

Figure 6: Mean acceleration required during a station keeping flyaround to a tumbling target at different distances adn target's angular rates.

illumination condition at capture. It is worth noticing that poor illumination conditions do not prevent the successful completion of capture, since the proximity operations can be planned in time accordingly or specific sensors can be employed which overcome this difficulties. However, it will impose additional constraints from the mission analysis and system design point of view which can be of relevant influence in the mission design process. The mass dependency is introduced as a simple linear inverse proportionality weighting the largest masses as the more problematic to be captured, considering an M_0 in Equation 9 equal to 10 tons.

6. MISSION RELATED INDEX

The fourth and last sub-index describes the impact of the objects orbit to the overall ADR mission requirements. The mission related index definition is as follows:

$$I_{mis} = \frac{N_{multi}}{150} + \frac{\Delta V_0 - \Delta V}{\Delta V_0} \qquad (11)$$

where

$$N_{multi} = \sum_j \left(h_j \in |\overline{h} \pm \Delta h| \right) \wedge \left(i_j \in |\overline{i} \pm \Delta i| \right) \wedge \left(M_j \in |\overline{M} \pm \Delta M| \right) \qquad (12)$$

where N_{multi} evaluates, for each candidate in the population, the number of similar objects in an altitude and inclination bin of dimension 100 km and 1 deg respectively and with a mass within $\pm$ 30% of its mass. In addition, a monotonically decreasing term function of the ΔV required to reach the target object is included. The estimation of the ΔV is preliminary computed considering an Hohmann transfer from a parking orbit with 400 km of altitude and same inclination as the target object to the target orbit. To relatively weight the sum of the two different terms, N_{multi} is normalised over the value of 150 while the ΔV is normalised considering the maximum value of reaching an altitude of 2000 km.

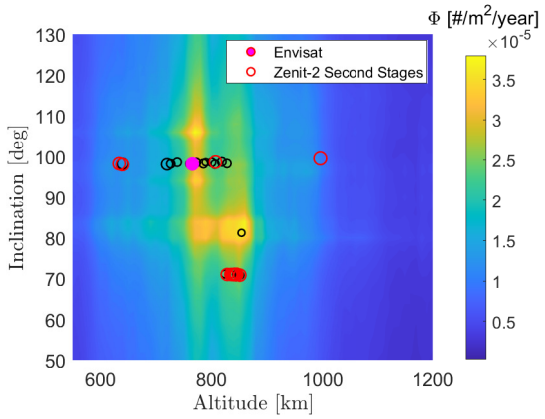

Figure 7: Scatter plot of the first 50 ranked objects in LEO. Color map represents the debris flux computed with MASTER-8.

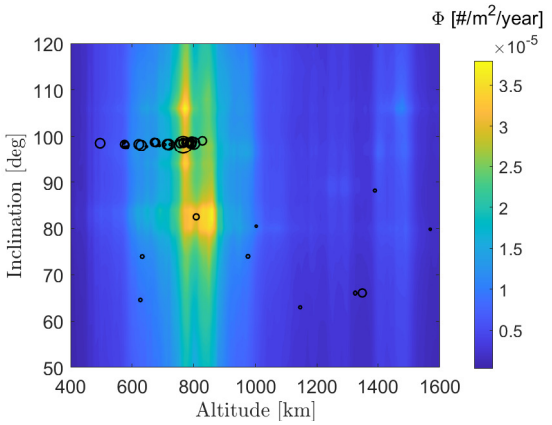

Figure 8: Scatter plot of the ESA owned object in LEO. Color map represents the debris flux computed with MASTER-8.

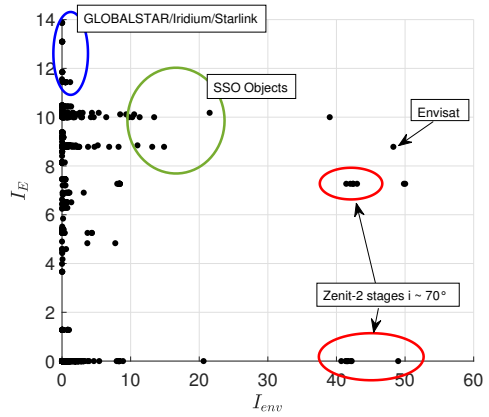

Figure 9: ADR candidates distribution in the (I_{env}, I_E) space for the analysed LEO population.

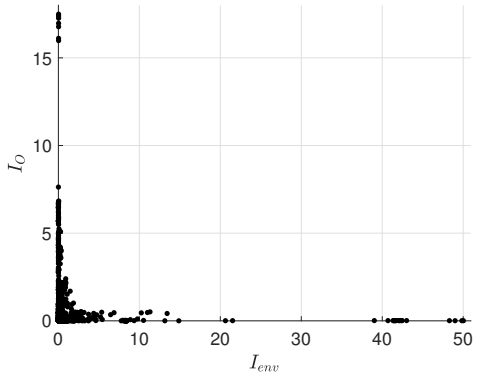

Figure 10: ADR candidates distribution in the (I_{env}, I_O) space for the analysed LEO population.

7. RANKING RESULTS FOR LEO

In this section the results of the application of the proposed ranking framework to the LEO debris population are presented and discussed. The population analysed comprehends payload and rocket bodies with mass greater than 100 kg in the region between 400 km and 2000 km of mean altitude.

The weights defined in the ADR index in Equation 1 are considered as follows: $w_{env} = 1$, $w_E = 1/5$, $w_O = 1/5$ and $w_{mis} = 1/2$. The peculiar choices are dictated both by the relative importance given to the different sub-indeces in the context of a general debris remediation mission, and from the fidelity of the employed model for the assessment. In the cases where the ADR service is designed to specific needs the weights can be adjusted accordingly. An example is the case of a commercial ADR service provided to satellite operators, where the remediation and reduction of collision risk and collision avoidance manoeuvres frequency in the orbital region of more economical resource values may be prioritized, thus the economical index weight would increase.

Table 2 reports the top ranking objects obtained from the ranking framework application to the LEO population. The first 50 objects are also displayed in the altitude and inclination space in Figure 7, where the object circle radius is proportional to the objects' mass. Two main regions can be identified as critical in LEO, namely the SSO region and the 70 deg inclination band around 800-900 km of mean altitude. In the top ranking spots most of the objects, as reported in Table 2 are of Russian ownership. In particular, massive Zenit-2 second stage residing in the 70 deg inclination band occupy most of the first positions.

In Figure 9 the distribution of the environmental index I_{env} and economical index I_E is shown for the objects analysed. It is interesting to note that some objects, although showing an extremely high value of environmental index, do not occupy highly valuable orbital regions in terms of economical resources, i.e. some Zenit-2 second stages at 70 deg of inclination. On the other hand, the highest scoring candidates from the economical in-

dex point of view, are the one associated to the highly valuable and populated regions of LEO constellations, even though scoring a very low environmental index impact. Some objects are also present which have the highest combined score in the distribution plot shown in Figure 9, i.e. Envisat and other objects in SSO. Figure 10 displays the distribution of environmental and operability index for the objects analysed. In this case, a quite inverse proportionality of the two index score is present, due to the inverse dependency of the two indeces with the objects' mass.

In general, most of the highest ranking objects are either of Russian or Chinese ownership. However, in the debris remediation missions, political requirements may be applicable where the close approach to other countries objects may be forbidden. Therefore, also the ranking list associated to only ESA states owned objects is reported in Table 3. Other than ENVISAT, for which the scientifici community awareness has already matured and several studies performed, the other objects are in general much down the overall list of priority. In Figure 8 are shown the distribution in mean altitude and inclination of the ESA states objects, where the circle's size represent the objects mass. Nonetheless, the European ranking still provides a priority list for candidate objects of a solely European ADR mission.

8. CONCLUSIONS

In this study, a framework to analyse the debris population and generate a priority list for removal was developed. Additionally to the assessment of the criticality of an object to the debris environment, a comprehensive quantification of several impact factors have been included in the ranking, i.e. economical resource value of orbital region, operability and mission related constraints. The ranking scheme was applied to the LEO debris population. Thanks to the multi-criteria method employed highlighted several different characteristics of the debris population which can be prioritized in the design of different ADR service, i.e. economical resource values for commercial services or operability constraints for low cost demonstration missions.

ACKNOWLEDGMENTS

The research leading to these results has received funding from the European Research Council (ERC) under the European Union Horizon 2020 research and innnovation program as part of the project COMPASS (Grant agreement No. 679086). www.compass.polimi.it.

REFERENCES

1. MMT Telescope Light Curves. http://mmt9.ru/satellites/. Accessed: 2020-12-01.

2. Allworth, J., Windrim, L., Wardman, J., Kucharski, D., Bennett, J., and Bryson, M. (2020). Development of a high fidelity simulator for generalised photometric based space object classification using machine learning. *arXiv preprint arXiv:2004.12270*.

3. Anselmo, L. and Pardini, C. (2015). Compliance of the italian satellites in low earth orbit with the end-of-life disposal guidelines for space debris mitigation and ranking of their long-term criticality for the environment. *Acta Astronautica*, 114:93–100.

4. Anselmo, L. and Pardini, C. (2016). Ranking upper stages in low earth orbit for active removal. *Acta Astronautica*, 122:19–27.

5. Anselmo, L. and Pardini, C. (2017). An index for ranking active debris removal targets in leo. In *Proc. 7th European Conference on Space Debris*, Darmstadt, Germany.

6. Biesbroek, R., Innocenti, L., Wolahan, A., and Serrano, S. M. (2017). e.Deorbit - ESA's Active Debris Removal Mission. In *Proc. 7th European Conference on Space Debris*.

7. Blackerby, C., Okamoto, A., Fujimoto, K., Okada, N., Forshaw, J. L., and Auburn, J. (2018). Elsa-D: an in-Orbit End-of-Life Demonstration Mission. In *Proceedings of the International Astronautical Congress, IAC*.

8. Blacketer, L. D. J., Lewis, H. G., and Urrutxua, H. (2019). A Technique for Rotation Vector Position Determination for Tumbling Rocket Bodies. In *First International Orbital Debris Conference*.

9. Brettle, H., Forshaw, J., Auburn, J., Blackerby, C., and Okada, N. (2019). Toward a Future Removal Service: Evolution of an ADR Business Model. In *Proceedings of the 70th International Astronautical Congress (IAC)*.

10. Colombo, C. (2016). Planetary orbital dynamics (PlanODyn) suite for long term propagation in perturbed envirnoment. In *Proceedings of the 6th International Conference on Astrodynamics Tools and Techniques (ICATT) (2016)*.

11. Colombo, C., Huang, S., Borelli, G., Cavenago, F., Nugnes, M., Gonzalo, J. L., Gaias, G., Massari, M., Vallini, L., Petit, M., Guerrieri, P., Valli, M., and Antonetti, S. (2021). Mission analysis and design for an active debris removal service for large constellations. In *8th European Conference on Space Debris*.

12. Colombo, C., Letizia, F., Trisolini, M., Lewis, H. G., Chanoine, A., Duvernois, P.-a., Austin, J., and Lemmens, S. (2017). Life cycle assessment indicator for space debris. In *7th European Conference on Space Debris*.

13. Dolgopolov, A., Smith, P., Stroup, T., Christensen, C., and Starzyk, J. (2020). Analysis of the Commercial Satellite Industry , Key Indicators and Global Trends. In *ASCEND Conference*, Virtual Event.

14. Floher, T., Lemmens, S., Bastida Virgili, B., Krag, H., Klinkrad, H., Parilla, E., Sanchez, N., Oliveira, J., and Pina, F. (2013). Discos – current status and future developments. *Proceedings of the 6h European Conference on Space Debris, ESOC, Darmstadt, Germany*, 2013(August):1–7.

Table 2: First 70 objects ranked by the ADR index I_{ADR} in the LEO region.

Norad	Type	Name	Mass [kg]	Country	h [km]	i [deg]	$\mathbf{I_{env}}$	$\mathbf{I_E}$	$\mathbf{I_O}$	$\mathbf{I_{mis}}$	$\mathbf{I_{ADR}}$
28353	RB	Zenit-2 second stage	9000.0	RUS	845	71.00	50.02	0.007	7.27	0.801	51.88
31793	RB	Zenit-2 second stage	9000.0	RUS	844	70.98	49.83	0.007	7.27	0.802	51.69
27386	PL	Envisat	8110.0	ESA	765	98.14	48.29	0.008	8.78	0.748	50.43
26070	RB	Zenit-2 second stage	9000.0	RUS	841	71.00	49.00	0.007	0.00	0.804	49.40
24298	RB	Zenit-2 second stage	8226.0	RUS	851	70.84	43.00	0.014	7.27	0.797	44.86
20625	RB	Zenit-2 second stage	8226.0	RUS	844	71.00	42.43	0.014	7.27	0.802	44.29
23088	RB	Zenit-2 second stage	8226.0	RUS	844	71.00	42.41	0.013	7.27	0.802	44.27
23405	RB	Zenit-2 second stage	8226.0	RUS	842	70.98	42.02	0.013	7.27	0.804	43.88
22803	RB	Zenit-2 second stage	8226.0	RUS	836	70.99	41.43	0.013	7.27	0.807	43.29
22566	RB	Zenit-2 second stage	8226.0	RUS	843	71.01	42.22	0.014	0.00	0.803	42.63
23705	RB	Zenit-2 second stage	8226.0	RUS	842	71.02	42.11	0.014	0.00	0.803	42.51
19650	RB	Zenit-2 second stage	8226.0	RUS	840	71.00	41.67	0.013	0.00	0.805	42.07
25407	RB	Zenit-2 second stage	8226.0	RUS	840	71.01	41.66	0.012	0.00	0.805	42.07
16182	RB	Zenit-2 second stage	8226.0	RUS	838	71.00	41.56	0.014	0.00	0.806	41.97
22220	RB	Zenit-2 second stage	8226.0	RUS	837	71.00	41.52	0.012	0.00	0.806	41.92
17590	RB	Zenit-2 second stage	8226.0	RUS	836	71.00	41.44	0.013	0.00	0.807	41.85
17974	RB	Zenit-2 second stage	8226.0	RUS	835	71.01	41.34	0.012	0.00	0.808	41.74
25400	RB	Zenit-2 second stage	8226.0	RUS	807	98.61	39.02	0.013	10.00	0.720	41.38
19120	RB	Zenit-2 second stage	8226.0	RUS	828	71.01	40.70	0.012	0.00	0.813	41.11
33272	PL	Cosmos-2441	7000.0	RUS	720	98.06	21.52	0.010	10.18	0.779	23.94
27006	RB	Zenit-2 second stage	9000.0	RUS	996	99.49	20.63	0.007	0.00	0.595	20.93
41858	RB	L-53 (YF24B)	4006.0	China	772	98.48	14.87	0.000	8.78	0.737	17.00
27601	RB	H-II LE-5B (H-IIA 202)	4000.0	Japan	785	98.22	13.43	0.419	10.00	0.728	15.88
44548	RB	L-53 (YF24B)	4000.0	China	761	98.13	13.15	0.002	8.78	0.745	15.28
37932	RB	L-53 (YF24B)	4006.0	China	819	98.66	11.31	0.511	10.00	0.706	13.77
31114	RB	L-55 (YF24)	3800.0	China	828	98.25	10.99	0.474	8.84	0.700	13.21
25860	PL	Okean-O	6300.0	RUS	640	98.21	10.52	0.024	10.12	0.835	12.96
28480	RB	L-55 (YF24)	3800.0	China	806	98.07	10.24	0.454	10.00	0.714	12.69
27597	PL	Midori-2 (Adeos 2)	3680.0	Japan	800	98.53	9.76	0.107	10.00	0.718	12.14
23343	RB	Zenit-2 second stage	8226.0	RUS	639	97.99	9.35	0.011	10.12	0.848	11.80
25861	RB	Zenit-2 second stage	8300.0	RUS	634	98.21	8.47	0.011	10.12	0.852	10.92
45722	RB	L-55 (YF24)	3800.0	China	738	98.55	8.24	0.001	8.78	0.760	10.38
17589	PL	Cosmos-1833	3221.0	RUS	850	70.91	8.45	0.000	7.27	0.685	10.25
22802	PL	Cosmos-2263	3221.0	RUS	849	70.92	8.41	0.000	7.27	0.686	10.21
22284	PL	Cosmos-2227	3221.0	RUS	848	70.98	8.40	0.000	7.27	0.686	10.20
23704	PL	Cosmos-2322	3221.0	RUS	848	70.99	8.39	0.000	7.27	0.693	10.19
16181	PL	Cosmos-1697	3221.0	RUS	848	70.97	8.39	0.000	7.27	0.686	10.19
24297	PL	Cosmos-2333	3221.0	RUS	848	70.91	8.39	0.000	7.27	0.686	10.18
22565	PL	Cosmos-2237	3221.0	RUS	851	70.84	8.33	0.000	7.27	0.684	10.12
26069	PL	Cosmos-2369	3200.0	RUS	848	71.00	8.30	0.032	7.27	0.699	10.11
17973	PL	Cosmos-1844	3221.0	RUS	845	70.90	8.28	0.000	7.27	0.688	10.08
25406	PL	Cosmos-2360	3171.5	RUS	851	70.81	8.05	0.000	7.27	0.684	9.85
11165	PL	Cosmos-1066	2725.5	RUS	854	81.23	8.89	0.066	0.00	0.689	9.25
36089	RB	L-55 (YF24)	3800.0	China	726	98.17	6.87	0.464	8.78	0.768	9.10
15755	PL	Cosmos-1656	3221.0	RUS	824	71.11	7.76	0.000	4.83	0.702	9.08
23710	PL	Radarsat	2724.5	Canada	789	98.57	6.44	0.351	10.00	0.725	8.88
23404	PL	Cosmos-2297	3221.0	RUS	847	71.01	8.38	0.000	0.00	0.686	8.72
22219	PL	Cosmos-2219	3221.0	RUS	847	71.06	8.37	0.000	0.00	0.687	8.72
23087	PL	Cosmos-2278	3221.0	RUS	846	71.06	8.35	0.000	0.00	0.687	8.69
15333	PL	Cosmos-1603	3221.0	RUS	845	71.03	8.30	0.000	0.00	0.688	8.65
20624	PL	Cosmos-2082	3221.0	RUS	845	71.04	8.27	0.000	0.00	0.688	8.62
19649	PL	Cosmos-1980	3221.0	RUS	843	71.00	8.22	0.000	0.00	0.689	8.56
19119	PL	Cosmos-1943	3221.0	RUS	842	71.00	8.16	0.000	0.00	0.690	8.50
28352	PL	Cosmos-2406	3200.0	RUS	854	71.00	7.96	0.032	0.00	0.695	8.32
39203	RB	L-55 (YF24)	3800.0	China	710	98.47	5.35	0.490	10.18	0.780	7.87
25634	PL	ARGOS	2490.0	US	828	98.45	5.21	0.216	8.84	0.700	7.37
25394	PL	Resurs-O1 N4	2444.0	RUS	811	98.68	4.63	0.015	10.00	0.718	6.99
21574	PL	ERS-1	2140.7	ESA	766	98.61	4.73	0.343	8.78	0.748	6.93
43610	RB	L-55 (YF24)	3800.0	China	713	98.56	4.36	0.426	10.18	0.778	6.87
24277	PL	Midori (ADEOS 1)	2468.8	Japan	794	98.89	4.21	0.196	10.00	0.722	6.61
27840	RB	Briz-KM (Rokot-KM)	1950.0	RUS	762	98.34	3.79	0.142	8.78	0.750	5.95
6276	RB	Star 26B (Thor-Burner IIA)	115.0	US	821	98.55	0.02	17.262	10.00	0.704	5.83
41580	RB	Briz-KM (Rokot-KM)	2370.0	RUS	809	99.09	4.36	0.142	5.25	0.726	5.80
44518	RB	Briz-KM (Rokot-KM)	2370.0	RUS	810	99.20	4.34	0.248	5.25	0.725	5.80
5904	RB	Star 26B (Thor-Burner IIA)	115.0	US	814	98.90	0.02	16.971	10.00	0.709	5.77
3158	PL	Cosmos-209 (NPP)	3800.0	RUS	902	65.33	5.42	0.074	0.00	0.664	5.77
7412	RB	Star 26B (Thor-Burner IIA)	115.0	US	816	98.76	0.02	16.776	10.00	0.708	5.73
6788	RB	Star 26B (Thor-Burner IIA)	115.0	US	805	98.87	0.02	16.115	10.00	0.715	5.60

Table 3: Ranking of ESA states objects in LEO.

Norad	Type	Name	Mass [kg]	Country	h [km]	i [deg]	I_{env}	I_E	I_O	I_{mis}	I_{ADR}
27386	PL	Envisat	8110	ESA	765	98.14	48.294	0.008	8.78	0.748	50.43
27597	PL	Midori-2 (Adeos 2)	3680	Jap/CNES	800	98.53	9.760	0.107	10.00	0.718	12.14
23710	PL	Radarsat	2724	Canada	789	98.57	6.444	0.351	10.00	0.725	8.88
21574	PL	ERS-1	2141	ESA	766	98.61	4.730	0.343	8.78	0.748	6.93
24277	PL	Midori (ADEOS 1)	2469	Jap/CNES	794	98.89	4.210	0.196	10.00	0.722	6.61
25261	RB	H10 (Ariane 40 H10)	1764	ESA	779	98.70	2.908	0.482	10.00	0.779	5.39
27422	RB	H10 (Ariane 42P H10)	1820	ESA	794	98.37	2.880	0.442	10.00	0.769	5.35
22830	RB	H10 (Ariane 40 H10)	1764	ESA	787	98.75	2.785	0.528	10.00	0.774	5.28
27421	PL	SPOT 5	3000	ESA	719	98.26	2.576	0.310	10.18	0.793	5.07
22823	PL	SPOT 3	1891	ESA	828	99.08	3.164	0.479	6.90	0.706	4.99
23561	RB	H10+ (Ariane 40 H10+)	1764	ESA	765	98.71	2.325	0.479	8.78	0.788	4.57
20443	RB	H10 (Ariane 40 H10)	1764	ESA	765	98.56	2.307	0.480	8.78	0.789	4.55
16615	RB	H8 (Ariane 1)	1318	ESA	786	98.47	1.623	0.664	10.00	0.741	4.13
25260	PL	SPOT 4	2730	ESA	714	98.29	1.614	0.406	10.18	0.790	4.13
21610	RB	H10 (Ariane 40 H10)	1764	ESA	756	98.45	1.784	0.481	8.78	0.795	4.03
27387	RB	EPS L9 (Ariane 5G)	1190	ESA	772	98.62	1.455	1.691	8.78	0.751	3.93
25977	PL	Helios 1B	2544	ESA	622	98.30	1.139	0.795	10.44	0.848	3.81
28368	PL	Demeter	132	ESA	647	97.85	0.006	6.454	10.12	0.837	3.74
33315	PL	Choma (RapidEye-3)	152	ESA	575	97.68	0.001	5.687	10.44	0.907	3.68
33316	PL	Choros (RapidEye-4)	152	ESA	581	97.69	0.001	5.691	10.44	0.903	3.68
33312	PL	Mati (RapidEye-2)	152	ESA	579	97.68	0.001	5.683	10.44	0.904	3.68
33313	PL	Trochia (RapidEye-5)	152	ESA	584	97.68	0.002	5.687	10.44	0.900	3.68
33314	PL	Tachys (RapidEye-1)	152	ESA	583	97.70	0.002	5.683	10.44	0.901	3.68
28499	RB	EPS L10 (Ariane 5G+)	2900	ESA	629	98.06	0.774	1.057	10.12	0.842	3.43
28498	PL	Parasol	110	ESA	665	98.34	0.006	4.397	10.12	0.817	3.32
28891	PL	Topsat	115	ESA	689	98.05	0.005	3.965	10.18	0.808	3.24
16613	PL	SPOT 1	1814	ESA	677	98.69	0.311	0.461	10.18	0.816	2.85
20436	PL	SPOT 2	1814	ESA	672	98.75	0.299	0.487	10.12	0.819	2.83
23608	RB	H10 (Ariane 40 H10)	1764	ESA	575	98.32	0.045	0.459	10.44	0.887	2.67
23560	PL	ERS-2	2494	ESA	496	98.55	0.034	0.290	10.48	0.937	2.66
25979	RB	H10 (Ariane 40 H10)	1240	ESA	579	98.14	0.019	0.480	10.44	0.877	2.64
36599	PL	PRISMA-Mango	150	ESA	706	98.24	0.010	0.637	10.18	0.796	2.57
36598	PL	Picard	150	ESA	724	98.32	0.008	0.006	10.18	0.783	2.44
40698	RB	AVUM (Vega)	170	ESA	573	98.65	0.000	0.014	9.17	0.882	2.28
22079	RB	H10 (Ariane 42P H10)	1764	ESA	1350	66.06	0.261	0.457	6.28	0.374	1.80
26997	PL	Jason	500	ESA	1326	66.04	0.030	0.300	6.28	0.389	1.54
25693	PL	UoSAT-12 (UO-36)	325	ESA	627	64.56	0.031	0.000	4.47	0.837	1.34
5104	PL	ISIS 2	262	Canada	1391	88.15	0.019	4.870	0.00	0.343	1.16
7003	PL	Aureole 2	396	ESA	633	73.92	0.005	3.613	0.00	0.840	1.15
5729	PL	Aureole 1	396	ESA	976	73.96	0.017	3.759	0.00	0.608	1.07
12848	PL	Aureole 3	991	ESA	808	82.48	0.157	2.013	0.00	0.720	0.92
424	PL	Alouette 1	143	Canada	1003	80.47	0.014	0.000	0.00	0.584	0.31
22161	PL	Freja	257	ESA	1145	62.97	0.007	0.189	0.00	0.500	0.29
1804	PL	Alouette 2	144	Canada	1569	79.80	0.003	0.000	0.00	0.238	0.12

15. Forshaw, J. L., Aglietti, G. S., Salmon, T., Retat, I., Hall, A., Chabot, T., Pisseloup, A., Tye, D., Bernal, C., Chaumette, F., Pollini, A., and Steyn, W. H. (2017). The removedebris adr mission: Launch from the ISS, operations and experimental timelines. *Proceedings of the International Astronautical Congress, IAC*.

16. Frey, S. and Lemmens, S. (2017). Status of the space environment: Current level of adherence to the space debris mitigation. *JBIS - Journal of the British Interplanetary Society*, 70(2-4):118–124.

17. Huang, S., Colombo, C., Gonzalo, J. L., Masserini, A., Nugnes, M., Vallini, L., and Petit, M. (2020). Preliminary mission analysis of active debris removal service for large constellations. In *Proceedings of the 71st International Astronautical Congress (IAC)*.

18. IADC (2002). Inter-Agency Space Debris Coordination Committee, Space Debris Mitigation Guidelines. (22):1–10.

19. Šilha, J., Pittet, J.-N., Hamara, M., and Schildknecht, T. (2018). Apparent rotation properties of space debris extracted from photometric measurements. *Advances in Space Research*, 61(3):844–861.

20. Johnson, N. L., Krisko, P. H., Liou, J. C., and Anz-Meador, P. D. (2001). NASA's new breakup model of EVOLVE 4.0. *Advances in Space Research*, 28(9):1377–1384.

21. Kaminski, K., Koshkin, N., Shakun, L., Golebiewska, J., Korobeinikova, E., and Wnuk, E. (2017). Determination of Orbital and Spin Parameters of Leo Satellites By Polish and Ukrainian Optical Observatories. *7th European Conference on Space Debris, Darmstadt, Germany, 18–21 April 2017*, (7(1)):N/A.

22. Kessler, D. J. and Cour-Palais, B. G. (1978). Collision Frequency of Artificial Satellites: the Creation of a Debris Belt. *J Geophys Res*, 83(A6):2637–2646.

23. Koshkin, N. I., Savanevich, V., Pohorelov, A., Shakun, L., Zhukov, V., Korobeynikova, E., Strakhova, S., Moskalenko, S., Kashuba, V., and Krasnoshchokov, A. (2017). Ukrainian Database and Atlas of Light Curves of Artificial Space Objects. *Odessa Astronomical Publications*, 30(0):226–229.

24. Kunstadter, C. (2021). Space Insurance and Collision Risk. In *1st MASTER Modelling Workshop*, ESA/ESOC.

25. Letizia, F., Colombo, C., Lewis, H. G., and Krag, H. (2016). Assessment of breakup severity on operational satellites. *Advances in Space Research*, 58(7):1255–1274.

26. Letizia, F., Colombo, C., Lewis, H. G., and Krag, H. (2017). Extending the ECOB Space Debris Index With Fragmentation Risk Estimation. *7th European Conference on Space Debris, Darmstadt, Germany*, (417):1–10.

27. Liou, J. C. (2011). An active debris removal parametric study for LEO environment remediation. *Advances in Space Research*, 47(11):1865–1876.

28. Liou, J. C. and Johnson, N. L. (2009). A sensitivity study of the effectiveness of active debris removal in LEO. *Acta Astronautica*, 64(2-3):236–243.

29. McKnight, D., Witner, R., Letizia, F., Lemmens, S., Anselmo, L., Pardini, C., Rossi, A., Kunstadter, C., Kawamoto, S., Aslanov, V., Dolado Perez, J. C., Ruch, V., Lewis, H., Nicolls, M., Jing, L., Dan, S., Dongfang, W., Baranov, A., and Grishko, D. (2021). Identifying the 50 statistically-most-concerning derelict objects in LEO. *Acta Astronautica*, 181(January):282–291.

30. Pittet, J. N., Silha, J., Schildknecht, T., Richard, M., Anal, H. D., Paccolat, C., Gass, V., and Thiran, J.-p. (2017). Space Debris Attitude Determination of Faint Leo Objects Using Photometry: Swisscube Cubesat Study Case. *Proc. of 7th European Conference on Space Debris, Darmstadt, Germany*, (June):18–21.

31. Rossi, A., Valsecchi, G. B., and Alessi, E. M. (2015). The criticality of spacecraft index. *Advances in Space Research*, 56(3):449–460.

32. Šilha, J., Krajčovič, S., Zigo, M., Tóth, J., Žilková, D., Zigo, P., Kornoš, L., Šimon, J., Schildknecht, T., Cordelli, E., Vananti, A., Mann, H. K., Rachman, A., Paccolat, C., and Flohrer, T. (2020). Space debris observations with the Slovak AGO70 telescope: Astrometry and light curves. *Advances in Space Research*, 65(8):2018–2035.

33. Silha, J., Schildknecht, T., Pittet, J., Kirchner, G., and Steindorfer, M. (2017). Debris Attitude Motion Measurements and Modelling by Combining Different Observation Techniques. In *Proc. 7th European Conference on Space Debris*, number June, Darmstadt, Germany.

34. Šilha, J., Schildknecht, T., Pittet, J. N., Rachman, A., and Hamara, M. (2017). Extensive light curve database of astronomical institute of the university of bern. In *Proc. of 7th European Conference on Space Debris*, Darmstadt, Germany.

35. Virgili, B., Lemmens, S., and Krag, H. (2014). Investigation on Envisat attitude motion. *ESA e.Deorbit Symposium*.

36. Virgili, B. B. and Krag, H. (2013a). Active Debris Removal For LEO Missions. In *Proc. 6th European Conference on Space Debris*, number April.

37. Virgili, B. B. and Krag, H. (2013b). Criteria for the Selection of Targets for Active Debris Removal. In *Proc. of 4th CEAS Air and Space Conference*.

38. Yasaka, T. (2011). Can we have an end to the debris issue? In *62nd International Astronautical Congress 2011, IAC 2011*, volume 3, pages 2197–2203.